FORMATION AND MICROSTRUCTURE EVOLUTION OF INTRACRYSTALLINE PORES IN LIGHTWEIGHT MICROPOROUS ALUMINA

Lvping Fu[1], Huazhi Gu[1], Ao Huang[1], Meijie Zhang[1], Zhengkun Li[2]

1) The State Key Laboratory of Refractories and Metallurgy, Wuhan University of Science and Technology, Wuhan 430081, China

2) Jiangsu Jingxin New Material Co., Ltd, Yangzhou 225265, China

ABSTRACT

The goal of designing a lightweight wear lining refractory for industrial furnaces has attracted increased attention in the field of refractory materials because a high-porosity lightweight wear lining could produce better heating insulation and thermal spalling resistance. In order to achieve guaranteed slag resistance of prepared lightweight wear lining, fabrication of refractory aggregates with high closed porosity, especially intracrystalline pores, has attracted increasing attention. In the present work, nano-alumina sol had been introduced to form a pile-up of nano–micro double-scale, and its effects on the properties and microstructure of prepared lightweight alumina was investigated. The introduction of nano-alumina sol led to the abnormal grain growth of prepared lightweight microporous alumina, and numerous straight line-distributed intracrystalline pores were observed inside of the abnormally-grew grains. Therefore, resulting in an increase in the closed porosity and decrease in bulk density. A mathematical model was proposed to investigate the formation and microstructure evolution of intracrystalline pores in lightweight microporous alumina. Calculation results showed that the nano–micro double-scale effect created partial regions in which the alumina sol collected, which showed a larger surface stress than other regions. Shrinkage occurred in the partial region simultaneously with grain growth, which led to the formation of intracrystalline cylindrical pores. Moreover, the introduction of nano-alumina sol resulted in a decrease in the closure time of cylindrical pores, then numerous straight line-distributed intracrystalline pores were formed.

Keywords： microstructure evolution, intracrystalline pores, lightweight microporous alumina, nano-alumina sol, pore closure

1. INTRODUCTION

For the demand of energy saving, heat insulation materials have been developed rapidly in recent years. A lightweight wear lining refractory has attracted increasing attention in the field of refractory materials. However, due to the introduction of pores, a poor slag resistance performance is always accompanied with the prepared lightweight materials. Hence, the key challenge in the development of lightweight wear lining refractories lies in achieving guaranteed resistance against slag corrosion [1].

Several researches have been carried out concerning on the slag resistance of porous refractory aggregates [2-4]. Huang et al. [3] pointed out that the miniaturization of pore size could improve the slag resistance of lightweight aggregate. The slag resistance mechanism of lightweight microporous aggregate has been proposed by Fu et al. [4], who studied the slag resistance performance of microporous corundum and tabular corundum. A continuous isolation layer was observed around the microporous corundum, which showed a significantly better slag resistance than tabular corundum. They also pointed out that the small pore size of microporous corundum aggregate would result in a formation of columnar crystals of $CaAl_{12}O_{19}$ (CA_6) and $CaAl_4O_7$ (CA_2), which was considered to be the main reason for the differences in slag resistance. Therefore, in order to improve the slag resistance of lightweight refractories, fabrication of refractory aggregates with high amount of closed pores, especially intracrystalline pores, and small pore size has been especially emphasized.

Brook [5] reported that pores would separate from the boundary when the migration velocity of the boundary became greater than that of the pores. That is, since open pores hinder boundary migration, if grain boundaries can move freely, then the pores are closed between the grain boundaries. As such, in this study, nano-alumina sol was introduced during the fabrication of microporous corundum aggregates. In this study, microporous alumina aggregates were obtained by adding nano-sized alumina sol to α-Al_2O_3 micropowder. Its effect on the sintering properties and microstructures of the microporous alumina aggregates was investigated.

2 EXPERIMENTAL

2.1 Raw materials

α-Al_2O_3 micropowder (D_{50}=2.36 μm, Kaifeng Special Refractory Co., Ltd., China) and nano-alumina sol (D_{50}=30 nm, solid loading was 25 wt%, Zibo Jinqi Chemical Technology Co., Ltd., China) were selected as raw materials and carbohydrate polymers (Shandong Hengren Industrial Trade Co., Ltd., China) as a binder and pore former.

2.2 Experimental procedure

The batch compositions of the samples are shown in Tab. 1. Carbohydrate polymer, with approximately 10 wt% of the raw materials, was added as an admixture. The raw materials and the carbohydrate polymer were mixed according to the batch compositions, and water, with approximately 40 wt% of the previously mentioned raw materials, was subsequently added in order to produce a slurry. The slurry was poured into the mold after 30 min wet milling with a planetary ball mill, solidified, and demolded. The microporous alumina was produced by drying the samples at 110 ℃ for 24 h and then heating at 1780 ℃ for 3 h.

Tab. 1: The batch compositions of samples (wt%)

Sample no.	S0	S1
α-Al_2O_3 micropowder	100	98.5
Solid content in nano-alumina sol	0	3
Carbohydrate polymer	10	10

2.3 Testing and characterization

The bulk density and apparent porosity were determined by Archimedes' Principle with water as the medium and the true density was measured using an automatic true density analyzer (ACCUPYC 1330, Micromeritics Instrument Corp., USA). In addition, the respective total and closed porosities of the samples were calculated from Eq. (1) and (2).

$$\pi_t = \frac{\rho_t - \rho_b}{\rho_t} \times 100\% \quad (1)$$

$$\pi_f = \pi_t - \pi_a \quad (2)$$

where π_t, ρ_t, ρ_b, π_a, and π_f are the total porosity, true density, bulk density, apparent porosity, and the closed porosity, respectively.

The samples were cut to sizes of approximately 5×5×5 mm^3 and then examined by Mercury Porosimetry (Autopore IV9500, Micromeritics Instrument Corporation, USA) in order to obtain the distribution of pore sizes. The thermal conductivities of samples were tested by laserflash thermal analyzer (Flashline TM 5000, Anter Corporation, USA). The microstructures and composition of the samples were characterized by scanning electron microscopy (SEM, Quanta 400, FEI Company, USA).

3 RESULTS

3.1 Physical properties

The physical properties of different samples are listed in Tab. 2. Compared to the unmodified sample, the sample containing nano-alumina sol showed a lower bulk density, higher closed porosity, lower apparent porosity, lower thermal conductivity, and smaller pore size.

Tab. 2: Physical properties of different samples

Sample no.	S0	S1
Bulk density/ g·cm^{-3}	3.32	3.25
Apparent porosity/ %	12.4	10.5
Closed porosity/ %	2.8	7.1
Total porosity/ %	15.2	17.6
Thermal conductivity at 800 °C/ W·m^{-1}·K^{-1}	7.53	6.32
Median pore diameter/ μm	1.26	0.69

3.2 Microstructure

Fig. 1 shows the SEM images of different samples. It can be seen that the majority of the grains in sample S0 were granular, and the size of grain was small, approximately 20 μm. The pores were uniformly distributed in the sample, however, most of them were distributed between the grain boundaries, rather than intracrystalline pores (Fig. 1(a)).

However, abnormal growth of the grains was observed in the sample containing nano-alumina sol. The size of the abnormally-grew grains was around 100~200 μm, and numerous intracrystalline pores, with a diameter of approximately 1 μm, were observed inside of them (Fig. 1(b)).

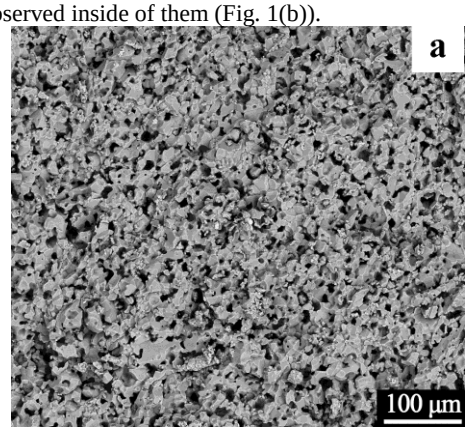

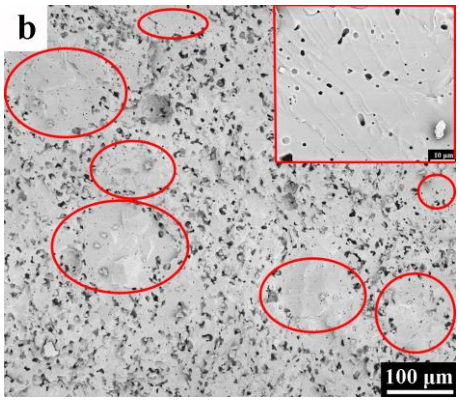

Fig. 1: SEM images of different samples: (a) S0; (b) S1

4 DISCUSSION

In this study, nano-alumina sol was introduced to form a pile-up of nano–micro double scales, and its effect on the properties and microstructure of lightweight microporous alumina was investigated.

The formation and elimination of pores in sintered materials is affected mainly by the migration velocities of grain boundaries and pores. Hence, the migration driving force of grain boundaries were calculated.

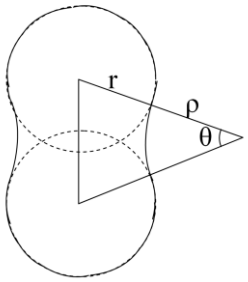

Fig. 2: The neck between two particles

As shown in Fig. 2, the surface stress in the neck between two semi-liquid particles can be calculated by the following equation [:6]:

$$P = \frac{\gamma_1}{\rho_1} + \frac{\gamma_2}{\rho_2} \tag{3}$$

where P is the surface stress, γ_1 and γ_2 are the surface energies, and ρ_1 and ρ_2 are the curvature radii of the neck of two particles, respectively.

The curvature radius of the neck, ρ, can be calculated by the following equation:

$$\rho = r[\sin^{-1}(\frac{\theta}{2}) - 1] \tag{4}$$

where r is the radius of the particle and θ is the central angle of the neck.

The surface energies of α-Al_2O_3 micropowder at different temperatures can be estimated using the following equation [7]:

$$r = (892 - 0.12T)/1000 \tag{5}$$

Since the radius of the nano-alumina sol is 1/78.7 that of α-Al_2O_3, its surface energy would be approximately 78.7 times that of α-Al_2O_3 micropowder.

Therefore, the surface stress in the neck between two α-Al_2O_3 micropowder particles and in the neck between one

α-Al_2O_3 micropowder particle and a nano-alumina sol particle can be obtained as follows:

$$P_1 = 1.149\times10^6 \times[\sin^{-1}(\frac{\theta}{2})-1]^{-1} \quad (6)$$

$$P_2 = 3.557\times10^9 \times[\sin^{-1}(\frac{\theta}{2})-1]^{-1} \quad (7)$$

where P_1 and P_2 are the surface stresses in the neck between two α-Al_2O_3 micropowder particles and in the neck between one α-Al_2O_3 micropowder particle and a nano-alumina sol particle, respectively, in units of Pa.

As shown in Eqs. (6) and (7), P_2 is 3.096×10^3 times of P_1. This indicates that the partial regions containing nano-alumina sol show larger surface stress.

In the process of sintering, pores can be regarded as a second phase that can restrain grain growth. As sintering continues, numerous very small pores disappear and the porosity of the sintered bulk decreases. When the sintering process has reached a certain degree, the remaining pores inside the sinter are sufficient to prevent further grain growth, and the grain sizes reach their limits. However, the introduction of nano-alumina sol produces a higher surface stress, indicating higher migration driving force of grain boundaries, which leads to the migration of grain boundaries. The grains simultaneously continue to grow and annex neighboring grains, the grain growth continues regardless of the inhibiting effect of the remaining trapped pores. The grain boundaries move freely during the grain growth process, and the pores are thus enclosed within the grains.

Stüwe et al. [8] found that the pores in doped tungsten wire would distributed practically in a straight line after drawing and annealing. They developed a dynamic model to describe the evolution of cylindrical pores into spheres. Similar phenomenon was also observed in our work. Fig. 3 shows the SEM image of a sample fabricated in this study. The arrangement of intracrystalline pores are almost in a row. Therefore, in this study, the formation of intracrystalline spherical pores are considered to follow the following evolution rules: the original cylindrical pores are closed by the grain boundaries, and then disintegrate into rows of small spheres. However, the integral intracrystalline pores in large grains are usually seemed to be randomly distributed. That is because their intracrystalline pores are evolved from numerous cylindrical pores, the randomly distribution of cylindrical pores results in randomly distributed intracrystalline pores. However, regional intracrystalline pores with a similar size are usually distributed in a row.

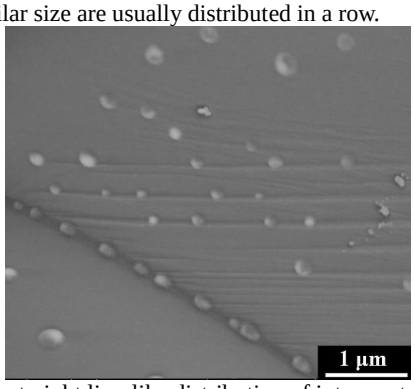

Fig. 3: The straight line-like distribution of intracrystalline pores

As such, the effect of nano-alumina sol on the disintegration of cylindrical pores into spheres are discussed in the following section.

Fig. 4 shows the evolution geometry of a cylindrical pore, with a radius of ρ, into a row of spherical pores, with a radius of R.

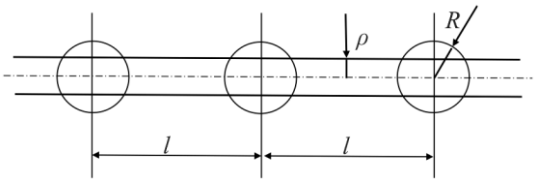

Fig. 4: The geometry of pores evolution

As shown in Fig. 5, the following equation is used to describe the fluctuation of the radius of cylindrical pore:

$$r = s + A\sin(\frac{2\pi}{l})x \quad (8)$$

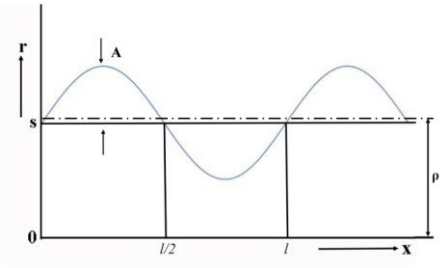

Fig. 5: The change of redius of near-cylinder pores

The disintegration of cylindrical pores into spheres can be considered as the diffusion of alumina molecules from the "bulge" to the adjacent "necks", as shown in Fig. 6. Then the change of fluctuation amplitude can be obtained based on Nernst-Einstein equation:

$$A(t) = A_0 \exp\left\{\frac{1}{2\nu\xi}\frac{D_s\gamma}{kT}(\frac{\psi}{\rho})^4 Zt\right\} \quad (9)$$

where A(t) is the fluctuation amplitude at the moment t; A_0 is the original fluctuation amplitude; v, ξ and Z are calculation parameters; D_s is the surface diffusion coefficient; γ is the surface energy; k is the boltzmann constant; T is the temperature; ψ is the diameter of alumina molecule; ρ is the radius of the cylindrical pore.

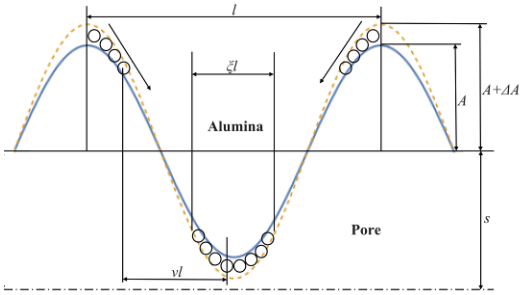

Fig. 6: The fluctuation of amplitude

When A(t)=ρ, the disintegration time of a cylindrical pore can be calculated with the following equation:

$$\tau = 2\nu\xi\frac{kT}{D_s\gamma}(\frac{\rho}{\psi})^4\frac{1}{Z}\ln\frac{\rho}{A_0} \quad (10)$$

The main parameters during the calculation are listed in Tab. 3. Introducing these parameters into equation (10), the closure time of cylindrical pores with or without nano-alumina sol addition can be then calculated. The introduction of nano-alumina sol could result in the closure time of cylindrical pores decrease from 1.58×10^4 to 1.18 hours.

Tab. 3: Main parameters during the calculation

Parameters	Value
Calculation parameter v	1/3 [8]
Geometrical parameter ξ	1/3 [8]
Boltzmann constant/ $J \cdot K^{-1}$	1.23×10^{-23} [8]
Temperature/ K	2053
Radius of the cylindrical pore/ m	10^{-7} [8]
Diameter of alumina molecule/ m	2×10^{-10} [5]
Calculation parameter Z	$1/(16\pi^2)$ [8]
Original fluctuation amplitude A_0/ m	2×10^{-10} [8]
Surface diffusion coefficient of α-Al_2O_3 micropowder/ $m^2 \cdot s^{-1}$	10^{-14} [9]
Surface diffusion coefficient of nano-alumina/ $m^2 \cdot s^{-1}$	8.518×10^{-13} [9]
Surface energy of α-Al_2O_3 micropowder/ $m^2 \cdot s^{-1}$	0.678 [7]
Surface energy of nano-alumina/ $m^2 \cdot s^{-1}$	53.359 [7]

Therefore, owing to the nano–micro double-scale effect, the partial regions containing nano-alumina sol showed larger surface stresses. The boundary migration velocities were increased, such that the cylindrical pores were closed before being eliminated. Moreover, the introduction of nano-alumina sol resulted in a decrease in the closure time of cylindrical pores, then the cylindrical pores were disintegrated into numerous straight line-distributed intracrystalline spherical pores.

5 CONCLUSIONS

The nano–micro double-scale effect created partial regions in which the alumina sol collected, which showed a larger surface stress than other regions. Shrinkage occurred in the partial region simultaneously with grain growth, which led to the formation of intracrystalline cylindrical pores. Moreover, the introduction of nano-alumina sol resulted in a decrease in the closure time of cylindrical pores, then numerous straight line-distributed intracrystalline pores were formed. Hence, the introduction of nano-alumina sol led to the abnormal grain growth of prepared lightweight microporous alumina, and numerous straight line-distributed intracrystalline pores were observed inside of the abnormally-grew grains. Therefore, resulting in an increase in the closed porosity and decrease in bulk density.

ACKNOWLEFGEMENTS

This work was supported by the National Natural Science Foundation of China (Grant no. 51474165).

REFERENCES

[1] Fu LP, Gu HZ, Huang A, Zhang MJ, Hong X Q, Jin LW. Possible improvements of alumina-magnesia castable by lightweight microporous aggregates. Ceram Int. 2015; 41 (1) 1263-70.

[2] Fu LP, Gu HZ, Huang A, Bai C. Effect of MgO micropowder on sintering properties and microstructures of microporous corundum aggregates. Ceram Int. 2015; 41 (4) 5857-62.

[3] Huang A, Gu HZ, Zou Y. Towards efficient modeling on slag corrosion of lightweight corundum spinel castable for ladle. In: Dana GG, Jeffrey DS, editors. UNITECR 2013: Proceeding of the 13th Unified International Technical Conference on Refractories; 2013 Sep 10-13; Victoria, BC, Canada. New Jersey: Wiley; 2013. p. 863-8.

[4] Fu LP, Gu HZ, Huang A, Zhang MJ, Li ZK. Slag resistance mechanism of lightweight microporous corundum aggregate. J Am Ceram Soc. 2015; 98 (5): 1658-63.

[5] Brook RJ. Pore-grain boundary interactions and grain growth. J Am Ceram Soc. 1969; 52 (1): 56–7.

[6] Burke JE. Role of grain boundaries in sintering. J Am Ceram Soc. 1957; 40 (3): 80–5.

[7] Rhee SK. Critical surface energies of Al_2O_3 and graphite. J Am Ceram Soc. 2006; 55 (6): 300–3.

[8] Stüwe HP, Kolednik O. Shape instability of thin cylinders. Acta Metall. 1988; 36 (7): 1705–8.

[9] Karasev VV, Onischuk AA, Glotov OG, Baklanov AM, Maryasov AG, Zarko VE, Panfilov VN, Levykin AI, Sabelfeld KK. Formation of charged aggregates of Al_2O_3, nanoparticles by combustion of aluminum droplets in air. Combust Flame. 2004; 138 (1-2): 40–54.